

# Surface-Functionalizable Plant-Derived Extracellular Vesicles for Targeted Drug Delivery Carrier Using Grapefruit

Kyunghwan Moon, Jihyeon Hur, Kwang Pyo Kim, Kangwon Lee,\* and Ji Yoon Kang\*

Recently, membrane-modified mammalian exosomes have been considered strong candidates for targeted drug delivery carriers because of their biocompatibility, biodistribution, and low immune response. However, the widespread utilization of exosomes still requires overcoming several challenging issues, including low stability, high production cost, and low mass productivity. Therefore, artificial extracellular vesicles (EVs) derived from cell membranes or liposomes containing various lipids have been suggested. However, only a few meet the demands of cost-effective mass production and durability of EVs. Therefore, this study investigates the feasibility of replacing mammalian cell exosomes and liposomes with plant-derived extracellular vesicles (pEVs) as targeted drug delivery carriers. They are characterized by nontoxicity, high stability, and high yield. Adding a functionalizable lipid moiety with a maleimide group at the membrane of grapefruit-derived pEVs imparts targeting ability. The targeting function can be easily enhanced by attaching an aptamer using click chemistry. Indeed, treatment of brain cells with pEV-aptamers (hCMEC/D3 and U87MG) confirms that aptamer functionalization of pEV enhanced selective cellular uptake. Functionalization of the pEV membrane using aptamer is expected to be effective in providing low-cost and mass-producible targeted drug delivery carriers with similar efficacy as mammalian exosomes or liposomes.

## 1. Introduction

Various methods for delivering drugs to the brain for treating diseases such as Alzheimer's disease and brain cancer, have been studied based on polymeric biomaterials, implanted scaffolds, and nanocarriers.<sup>[1–3]</sup> Among them, using nanoparticles or vesicles for drug delivery is mainly reported because it is less damaging to patients.<sup>[4]</sup> Notably, the drug needs to be able to traverse the blood–brain barrier (BBB) to reach the brain. The semipermeable BBB, which is critical to protecting the brain by providing a tight barrier to harmful substances, is composed of various cell types, including endothelial cells, astrocytes, pericytes, and microglia, all collaborating to maintain its integrity and function.<sup>[5]</sup> It restricts both large and small molecules (>400 Da) to block harmful substances and drugs in the bloodstream but allows nutrients to pass through.<sup>[6]</sup> Therefore, a drug delivery carrier must be capable of targeting

K. Moon, J. Y. Kang  
Brain Science Institute  
Korea Institute of Science and Technology  
Seoul 02792, Republic of Korea  
E-mail: jykang@kist.re.kr

K. Moon  
Program in Nanoscience and Technology  
Graduate School of Convergence Science and Technology  
Seoul National University  
Seoul 08826, Republic of Korea

J. Hur, K. P. Kim  
Department of Applied Chemistry  
Institute of Natural Science  
Global Center for Pharmaceutical Ingredient Materials  
Kyung Hee University  
Yongin 17104, Republic of Korea

K. P. Kim  
Department of Biomedical Science and Technology  
Kyung Hee Medical Science Research Institute  
Kyung Hee University  
Seoul 02453, Republic of Korea

K. Lee  
Department of Applied Bioengineering  
Graduate School of Convergence Science and Technology  
Seoul National University  
Seoul 08826, Republic of Korea  
E-mail: kangwonlee@snu.ac.kr

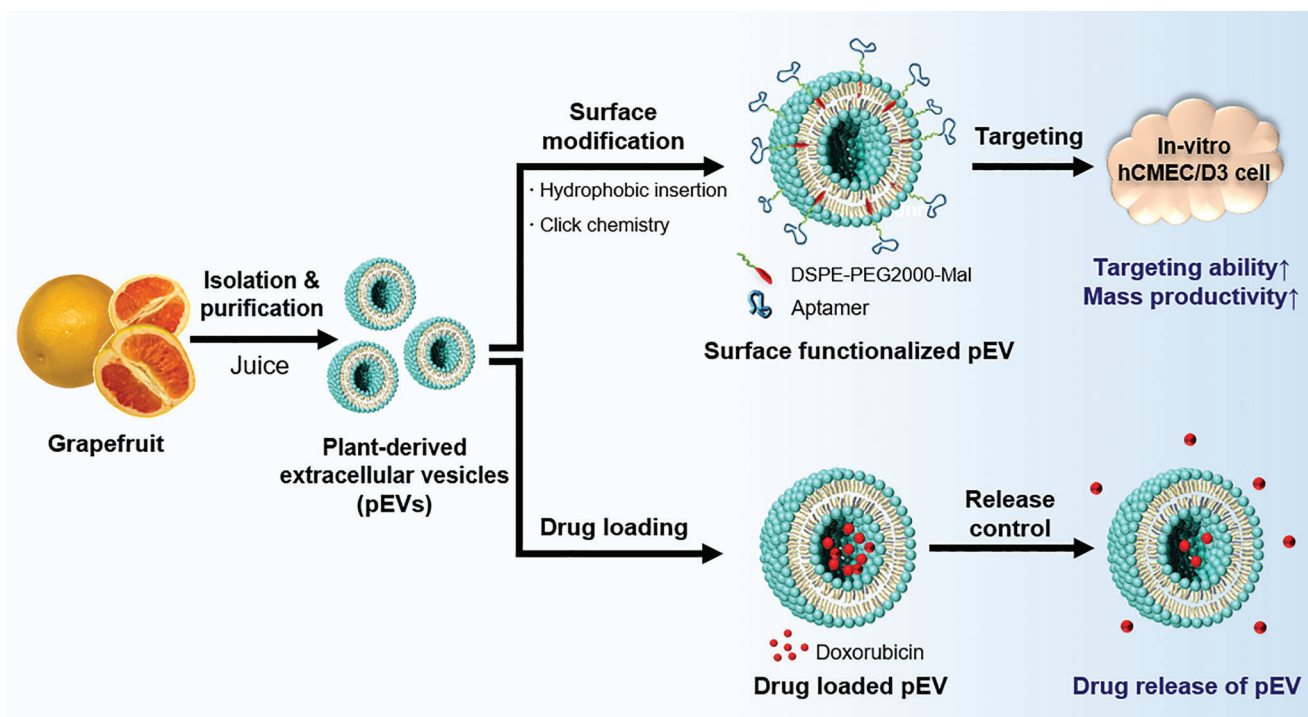
K. Lee  
Research Institute for Convergence Science  
Seoul National University  
Seoul 08826, Republic of Korea

J. Y. Kang  
Division of Bio-Medical Science and Technology  
University of Science and Technology  
Daejeon 34113, Republic of Korea

 The ORCID identification number(s) for the author(s) of this article can be found under <https://doi.org/10.1002/admi.202300220>

© 2023 The Authors. Advanced Materials Interfaces published by Wiley-VCH GmbH. This is an open access article under the terms of the Creative Commons Attribution License, which permits use, distribution and reproduction in any medium, provided the original work is properly cited.

DOI: 10.1002/admi.202300220



**Scheme 1.** Schematic illustration of the synthesis and treatment of surface modified plant-derived extracellular vesicles for a targeting delivery carrier and a drug loading carrier.

the cells constituting the BBB before passing through the BBB for efficient treatment of brain-associated disorders.

Exosomes are cell-derived extracellular vesicles (EVs) that are surrounded by a lipid bilayer and are 30–160 nm in diameter.<sup>[7]</sup> Their primary function is intercellular communication by delivering molecules such as miRNA, cytokines, and proteins, to other cells. Therefore, the ability of transporting molecules to other cells has been studied for use as nanocarriers during drug delivery.<sup>[8–10]</sup> Furthermore, some successful results have been demonstrated.<sup>[11]</sup> Recently, membrane-modified exosomes have been considered novel nanovesicle carriers for targeted drug delivery owing to their biocompatibility, biodistribution, and low immune response.<sup>[12–15]</sup> However, there are still several challenging issues associated with mammalian exosomes, including stability and homogeneity, as well as large-scale manufacturing.<sup>[16]</sup> Nanovesicles from cell membranes and liposomes from various lipids have been studied for use as artificial EVs to overcome these challenges. However, only a few meet the demands of cost-effective mass production, stability, and negligible side effects.<sup>[17,18]</sup>

As one of the efficient methods for drug delivery carriers, it was suggested to investigate the sources from plants and synthesize nature-friendly green nanocarriers. Recently, interest in nanomedicine research using plants has increased because of their biocompatibility, mass production, and low cost. Plant-derived extracellular vesicles (pEVs) are natural drug carriers with several advantages. They are characterized by high biocompatibility, low toxicity, uniformity, size of 50–300 nm, and negative surface charge. These features render them suitable drug carriers in various fields, such as health care, cosmetics, and biomedical

applications.<sup>[19]</sup> This study aimed to modify the surface of plant-derived extracellular vesicles to enhance their targeting ability and act as a drug delivery carrier.

The pEVs secreted from plant cells contain their metabolites within the lipid bilayer<sup>[20,21]</sup> and communicate with other cells using exosome-like interactions.<sup>[22]</sup> Recent reports have demonstrated that natural pEVs can circulate in the human body, showing good bioavailability. Accordingly, pEVs extracted from various plants were treated with various human cells to observe their effects as drugs.<sup>[23]</sup> Moreover, it has been reported that the cellular internalization of pEV is similar to that of existing mammalian-derived exosomes.<sup>[24,25]</sup> The pEV is considered similar to mammalian exosomes in terms of structure and composition. They are nontoxic nanovesicles that can be efficiently internalized into mammalian cells. Because pEVs are suitable for mass production with high yield and stability, they can replace animal exosomes for acting as drug delivery carriers. However, owing to differences in species' origin, pEV lacks the ability to target delivery in mammalian cells. This needs to be overcome to ensure a low-cost drug delivery system.<sup>[26]</sup>

We studied the feasibility of conferring BBB endothelial cell targeting ability to pEVs and whether they could act as targeted drug-delivery carriers. Furthermore, we assessed whether pEVs could function as drug-loading carriers using Doxorubicin as a model drug. Grapefruit was used as the plant source of pEVs (**Scheme 1**). Then, a functionalizable lipid moiety, maleimide-group-modified lipid, was inserted into the membrane of the pEVs for drug targeting.<sup>[27,28]</sup> The moiety at the pEV membrane was confirmed by colocalized fluorescence of DiO and Cy5-labeled lipids. The targeting function of the moiety can be easily

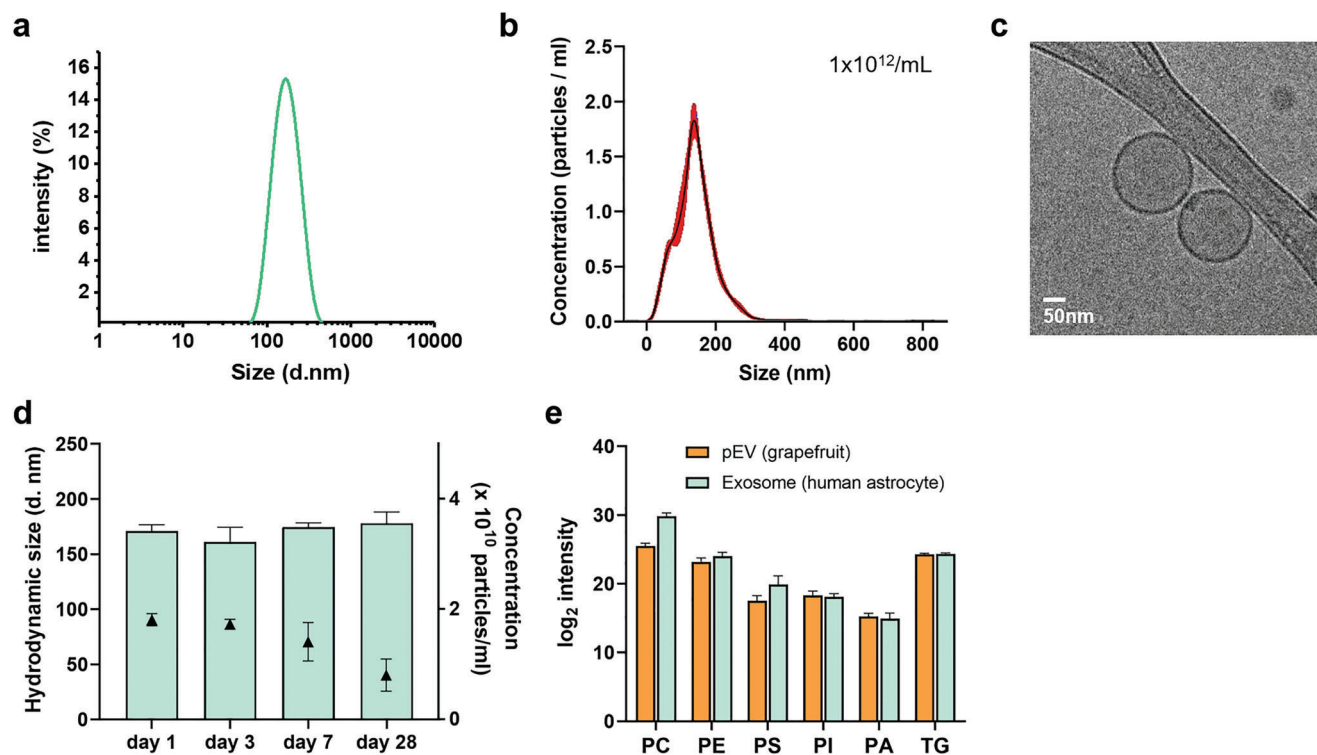


**Figure 1.** The characterization of pEVs isolated from grapefruit. a) The average hydrodynamic size and b) the concentration of pEV. c) Cryo-electron microscopy (Cryo-EM) images of pEVs. d) The stability of pEVs for 28 days. Change of hydrodynamic size and concentration of pEVs. e) comparison of lipidomic analysis results: lipids intensity of pEVs from grapefruit and exosomes from human astrocyte primary cell. (\*PC: Phosphatidylcholine, PE: phosphatidylethanolamine, PS: phosphatidylserine, PI: Phosphatidylinositol, PA: Phosphatidic acid, TG: Triglyceride) All bars represent means  $\pm$  SD ( $n = 3$ ).

enhanced using click chemistry. Notably, 3'-Thiol-modified R11-3 (CGAGUGCUUUUGAAUACUCUGGUUAGGGUCAUGCGGUUUG) aptamers targeting hCMCE/D3 BBB endothelial cells were used to confer targeting ability to pEV. The hCMCE/D3 cell line, which is the cell composition of the BBB model were used for in vitro analyses.<sup>[29]</sup> As a result, pEV with the aptamer was able to target a specific cell, confirming its potential as a drug delivery carrier. Moreover, its ability to function as a drug-loading carrier was also demonstrated. We expect that the functionalization of the pEV membrane will provide a low-cost target drug delivery carrier platform based on plant-derived source with similar efficacy as mammalian exosomes or liposomes with high stability and mass productivity. As far as we know, this is the initial research on modifying the surface of pEV to utilize it as a drug carrier that can be targeted.

## 2. Results and Discussion

### 2.1. Characterization of pEVs

Plant-derived extracellular vesicles were isolated from grapefruit juice. The average hydrodynamic diameter of pEV was  $170.9 \pm 5.7$  nm (Figure 1a). A total volume of 1.2 mL pEV was obtained at a concentration of about  $1 \times 10^{12}$  particles  $\text{mL}^{-1}$  from one grapefruit (Figure 1b). The size distribution of the pEVs from nanoparticle tracking analysis (NTA) showed that it was similar to that of previously reported exosomes.<sup>[30]</sup> The yields of pEVs

and exosomes were investigated by comparing the number of exosomes extracted from mammalian cells to plant-derived extracellular vesicles. The initial volume of exosomes was 50 mL, and the harvested particle number and volume of exosomes were about  $1 \times 10^{10}$   $\text{mL}^{-1}$  and 200  $\mu\text{L}$ , respectively. The pEV isolated from grapefruit juice with the same volume yielded about  $1 \times 10^{12}$   $\text{mL}^{-1}$  in 600  $\mu\text{L}$ , and the total particle number of EV was about 300 times higher than that of the exosomes (Figure S1, Supporting Information). The weight of the grapefruit was  $380 \pm 40$  g, and it was possible to obtain more than 120 mL of juice from each grapefruit (Figure S2, Supporting Information). Therefore, it is implied that a high yield of pEV is advantageous for commercialization owing to less labor and cost.

The cryo-EM image of pEV showed a size of approximately  $171 \pm 14$  nm, and the peak size distributions from dynamic light scattering (DLS) and NTA were in agreement (Figure 1c). The spherical morphology of pEV was similar to that of animal cell exosomes.<sup>[31]</sup> The stability of pEV was investigated for use as drug delivery carriers. When they were stored for 28 days in phosphate buffered saline (PBS) at 4 °C, no significant change in diameter was observed. The pEV concentration remained stable until 7 days but decreased to less than 1/2 after 28 days. It is roughly estimated that pEVs were stable until 1 week indicating excellent preservation (Figure 1d). Through the size range classification analysis, it was found that there were no considerable changes in the sizes distributions over time (Figure S3, Supporting Information). Lipidomic analysis was performed to investigate whether

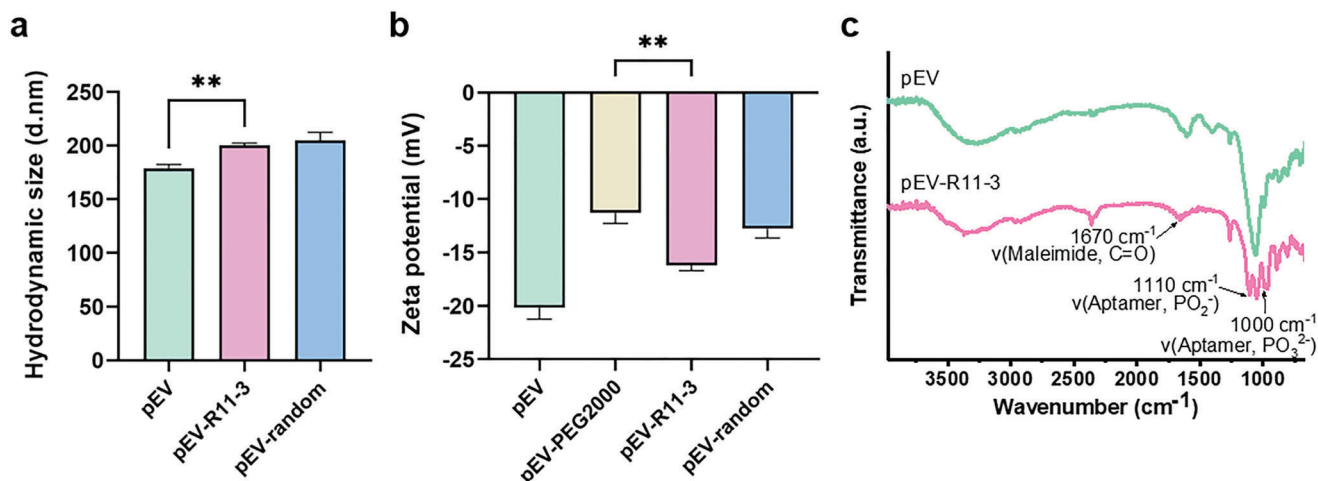


**Figure 2.** The identification of pEVs after surface functionalization. a) The average hydrodynamic size of pEVs and surface modified pEV-R11-3 and pEV-random sequence. b) Change of zeta potential of pEVs, pEV-PEG2000, and pEV-Aptamers. c) Fourier transform infrared spectroscopy (FT-IR) of pEVs and pEV-R11-3. All bars represent means  $\pm$  SD ( $n = 3$ ).  $**p < 0.01$ .

the membrane constituent lipids of the pEV were comparable to those of mammalian exosomes. The  $\log_2$  lipid intensity results showed that the lipids composition of the pEV was similar to mammalian exosomes (Figure 1e). There was a slight variation in the proportions of specific lipids, including PC, PE, PS, and TG, between pEV and mammalian exosomes. These findings suggest that pEV has a similar structure to mammalian-derived exosomes and exhibits high stability owing to its comparable lipid composition.

## 2.2. Surface Modification of pEVs

Because pEV is derived from a different species, unlike exosomes derived from animals, they cannot recognize and target a specific part of the human body. Therefore, it is essential to confer the ability to target to pEVs so they can be used as drug-delivery carriers in mammalian cells. Several methods have been studied for modifying the surface of exosomes and liposomes in mammals, including genetic engineering, incubation with parent cells, and hydrophobic interactions.<sup>[27]</sup> However, there has been limited research on surface modification of pEVs. In this study, specific lipids were inserted into the lipid bilayer of pEVs via hydrophobic interactions, modifying the surface to obtain the desired properties. In this study, a 1,2-distearoyl-sn-glycero-3-phosphoethanolamine (DSPE) lipid was inserted between the lipid bilayers of the pEV membrane using hydrophobic insertion to confer various targeting abilities.

The aptamer R11-3 is known to undergo cell internalization in endothelial cells through endocytosis and it has been studied for enabling transcytosis. The immobilization of the aptamer on the pEV surface was accomplished through the hydrophobic insertion of DSPE-PEG2000-Mal and click chemistry of the 3' thiol-modified aptamer. The surface-functionalized pEVs by R11-3 and random sequence aptamer showed an increase in sizes to  $204.9 \pm 7.55$  and  $200.6 \pm 3.63$  nm, respectively. The initial concentration of pEV was  $1 \times 10^{11}$  particles mL<sup>-1</sup> and decreased to about  $4 \times 10^{10}$  particles mL<sup>-1</sup> and  $2 \times 10^{10}$  particles mL<sup>-1</sup> following surface

treatment with the aptamers (Figure 2a). Thiol-AAAAA-Cy5 was used to confirm the hydrophobic insertion of DSPE-PEG2000-Mal to the membranes of pEV. They were then subjected to a click chemistry reaction after incubation for 2 h at 25 °C. The resulting pEV-DSPE-PEG2000-Cy5 was labeled with DiO, a green fluorescent dye, and observed using a confocal microscope. The co-localization of the fluorescent dyes DiO and Cy5 confirmed the insertion of DSPE into the membrane of pEV (Figure S4, Supporting Information). Zeta potential and Fourier transform infrared (FT-IR) spectroscopy indicated a significant change after aptamer modification. The surface charge of the pEV showed a negative potential, similar to the previously known properties of mammalian exosomes.<sup>[32]</sup> When R11-3 aptamer and random sequence aptamer were attached, the zeta potential increased from  $-20.16 \pm 1.07$  to  $-16.16 \pm 0.51$ , and  $-12.76 \pm 0.86$  mV, respectively (Figure 2b). In pEV-PEG2000, the presence of neutral polyethylene glycol (PEG) chains on the surface of the pEVs contributes to the reduction in negative charge. Following the conjugation of aptamers to the terminal of PEG chains via click chemistry, the negative charge of the pEV-Aptamer increases due to the negative charge of the nucleic acid content of the aptamer. The surface modification of pEV with the DSPE-PEG2000-aptamer using hydrophobic insertion was confirmed in the FT-IR spectrum (Figure 2c). The maleimide–thiol conjugates C=O peak at  $1670 \text{ cm}^{-1}$  originated from two carbonyls symmetric groups on maleimide five-membered ring.<sup>[33]</sup> and the PEG 2000 peaks approximately at  $1100 \text{ cm}^{-1}$ <sup>[34]</sup> appeared in the FT-IR spectrum. Additionally, the  $\text{PO}_2^-$  and  $\text{PO}_3^{2-}$  peaks of the aptamer phosphate backbone were observed at 1110 and  $1000 \text{ cm}^{-1}$ , respectively.

Consequently, DSPE-PEG2000-maleimide was chosen among the DSPE-PEG derivatives that could easily modify the surface of pEV quickly, and in high yields. The results of DLS and zeta potential measurements confirmed the surface modification of the pEV before conferring the targeting ability. As an additional function, PEG linked to the lipid acted as a biostability factor, allowing the pEV to exist for an extended period, avoiding protein binding to the pEV.<sup>[35]</sup> After inserting lipids on the surface of pEV, the thiol-modified R11-3 aptamer was attached through click

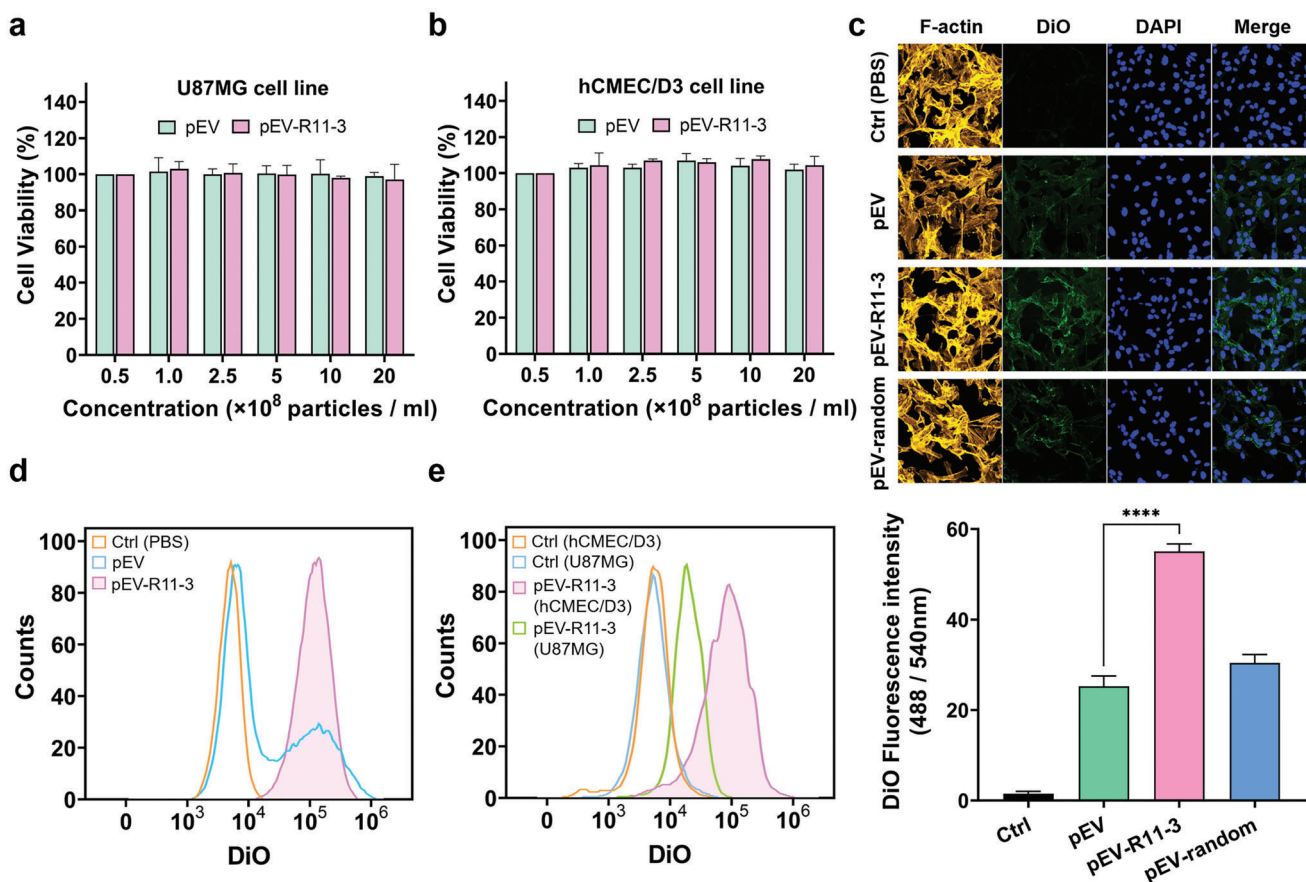


**Figure 3.** Cellular uptake of pEVs and cell viability analysis. a,b) The U87MG cell and hCMEC/D3 cell viability after incubation with pEV and pEV-R11-3 after 12 h. c) Confocal image and DiO fluorescence intensity quantification of confocal image using imageJ of hCMEC/D3 endothelial cell after DiO labeled pEV uptake (3 h). d,e) Fluorescence-activated cell sorting (FACS) of pEV, pEV-R11-3 incubated with hCMEC/D3 and U87MG cell line. All bars represent means  $\pm$  SD ( $n = 3$ ). \*\*\*\* $p < 0.0001$ .

chemistry between the maleimide and thiol groups. It was possible to connect aptamers to pEVs with ease and high yield to provide them with functional properties.

### 2.3. In Vitro Cellular Uptake of pEV-R11-3 into U87MG and hCMEC/D3 Cell Lines

The characterization of cellular uptake by pEVs and derivatives of pEVs into a glioblastoma U87MG and an endothelial hCMEC/D3 cell line were investigated because the internalization of pEVs was essential for using them as drug carriers. First, cytotoxicity was examined by cell viability test through treatment of pEV and pEV-R113 aptamers at various concentrations (0.5, 1.0, 2.5, 5, 10, and  $20 \times 10^8$  particles  $\text{mL}^{-1}$ ) for 12 h in the U87MG and hCMEC/D3 cell lines, respectively (Figure 3a,b). At all concentrations, neither pEV nor pEV-R11-3 showed cytotoxicity; cell viability was over 90% in both cell lines.

To visualize the cell-specific uptake of pEVs functionalized by the R11-3 aptamer (pEV-R11-3), a green fluorescent dye, DiO, was labeled on pEV, pEV-R11-3, and pEV functionalized by a random sequence aptamer (pEV-random). Then, U87MG and hCMEC/D3 cells were treated with these three pEV. The fluores-

cence of pEVs in the cells was viewed using confocal microscopy. After incubation of U87MG cells ( $1 \times 10^5$  cell per well) with pEV at a concentration of  $2 \times 10^9$  particles  $\text{mL}^{-1}$  the uptake of pEV at different incubation times (0.5, 1, 3, and 6 h) was analyzed via confocal microscopy. Fluorescence intensity increased with time and showed no significant differences after 3 h (Figure S5, Supporting Information). The pEV-R11-3 labeled with DiO fluorescent dye ( $2 \times 10^9$  particles  $\text{mL}^{-1}$ ) was incubated with the endothelial hCMEC/D3 cell line for 3 h until the cellular uptake of pEV was saturated. The pEVs with the R11-3 aptamer were internalized approximately twice as much in hCMEC/D3 cells than with untreated pEVs (Figure 3c), indicating that surface modification of pEVs using the R11-3 aptamer enhanced the cellular uptake of pEV.

Fluorescence-activated cell sorting (FACS) analysis was performed with hCMEC/D3 and U87MG cells treated with pEVs for 3 h to evaluate their targeting and internalization abilities. The results showed that the cells incubated with pEV-R11-3 aptamer showed higher fluorescence intensity than those incubated with pEV, as indicated by the significant peak shift to the right owing to the uptake of pEV-R11-3 by hCMEC/D3 cells (Figure 3d). The surface modification of pEV with the R11-3 aptamer through hydrophobic insertion enhanced cellular uptake. Furthermore,

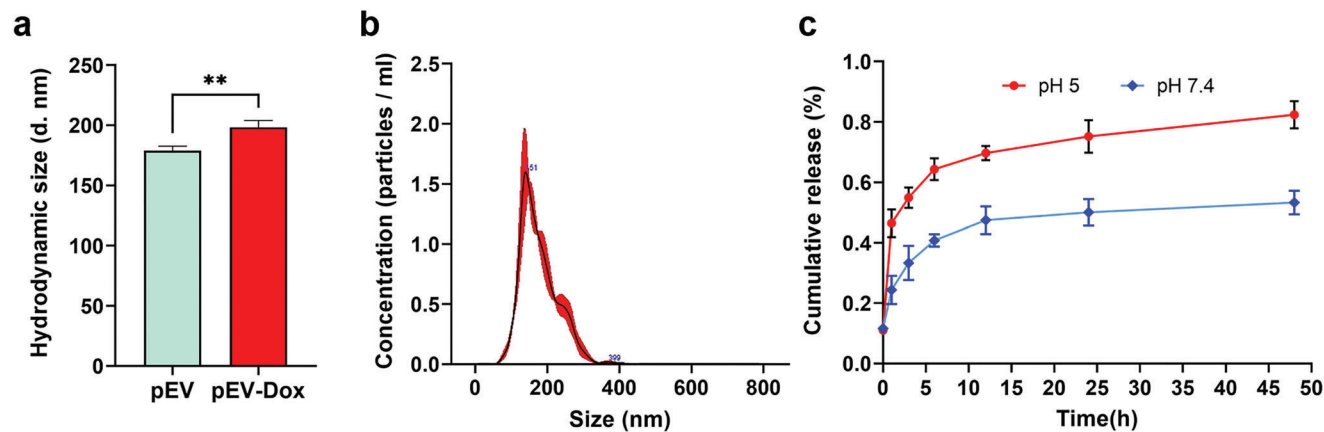


**Figure 4.** Doxorubicin loading and release of pEVs. a) The average hydrodynamic size of pEVs before and after drug loading. b) Concentration of pEV-Doxorubicin after Doxorubicin loading by probe sonication. c) The drug release profile of pEV-Doxorubicin in PBS at pH 5 and 7.4, respectively. All bars represent means  $\pm$  SD ( $n = 3$ ).  $**p < 0.01$ .

pEV-R11-3 was absorbed more in endothelial hCMEC/D3 cells than in glioblastoma U87MG cells (Figure 3e). pEV-R113 appears to have a higher affinity for endothelial cells than glioblastoma, implying that it can specifically target the brain endothelial cell line.<sup>[36]</sup> The targeting ability was conferred by the surface modification of pEV.

## 2.4. Drug Release

We characterized the kinetics of drug loading and release with pEV to investigate their potential use as drug carriers. As a model drug, doxorubicin was loaded into pEV by probe sonication, a physical drug-loading method. The size of the doxorubicin-loaded pEV was  $198.4 \pm 5.5$  nm, which is similar to that of pEV (Figure 4a,b). Drug release kinetics were studied under two different pH conditions (Figure 4c); pH 7.4 PBS, a physiological pH, and pH 5 PBS, an acidic environment such as the environment around cancer.<sup>[37]</sup> The pEV with doxorubicin showed bursts of release of up to 24% and 45% in the first 30 min at pH 7.4. Similar to a previous report on exosomes loaded with doxorubicin, its release from pEV was controlled by pH.<sup>[38]</sup> Approximately 45% of doxorubicin was released in 48 h at pH 7.4. In contrast, after an initial explosive release, drug release was  $\approx 80\%$  in 48 h under acidic pH 5 conditions. At pH 7.4, almost no more drug was released after the initial burst; however, at pH 5, an increasing trend was maintained for drug release up to 48 h.

The sustained release of the drug at pH 5 confirmed that the pEVs were capable of sustained release. The pEV could act as a drug delivery carrier and could load both hydrophilic and hydrophobic drugs owing to the lipid bilayer composition of pEV.<sup>[39]</sup>

## 3. Conclusion

Plant-derived extracellular vesicles were successfully extracted, and their surfaces were modified by inserting a lipid derivative (DSPE-PEG2000-Maleimide) into the pEV membrane through hydrophobic insertion. Thereafter, an aptamer (R11-3) with a

thiol group was attached to the surface of the modified pEV using click chemistry to enhance the targeting function of pEV. The enhanced cellular uptake of pEV with R11-3 into hCMEC/D3 confirmed that the aptamer (R11-3) bound to BBB endothelial cells with high affinity and increased the selectivity of pEV. This indicated that a novel targeted drug delivery carrier using plant-derived extracellular vesicles has been successfully developed. In addition, a drug release analysis with doxorubicin demonstrated that pEV could effectively control drug release. Further studies will be conducted to investigate targeted drug delivery carrier that can pass through the BBB.

In the future, the pEV-aptamer capable of targeted drug delivery will play a role as a low-cost, mass-produced, and biocompatible drug carrier based on a green manufacturing in the field of nanomedicine. Furthermore, when aptamers, proteins, miRNAs, and other biomolecules are attached to the pEV using surface modification with hydrophobic insertion and click chemistry, various cells or organs other than endothelial cells could be targeted. As a targeted drug carrier, the development of surface-functionalized pEV can be used in many applications of nanomedicine through further studies on the metabolism and mechanism of pEV in the human body.

## 4. Experimental Section

**Materials:** Grapefruit was purchased from Homeplus Grocery Store Ltd. (Seoul, Korea). 1,2-distearoyl-sn-glycero-3-phosphoethanolamine-*N*-[maleimide (polyethylene glycol)-2000](DSPE-PEG(2000) maleimide) and threo-1,4-Dimercapto-2,3-butanediol (DL-Dithiothreitol) were obtained from Sigma-Aldrich (St. Louis, MO). Sodium acetate, ethyl acetate, and dimethyl sulfoxide (DMSO) were obtained from Sigma-Aldrich (St. Louis, MO). Phosphate-buffered saline (PBS) was purchased from Welgene, Ltd. (Gyeongsan-si, Korea). R11-3 (3' Thiol Modified) Aptamer (CGAGUGCUUUUGAAUACUCUGGUUAGGGUCAUGCGUUUG) and random (3 thiol-modified) aptamer (AACUGCGGUAGCUUAAUUGAGAGCAUUCAAUGUUCUGAG) were synthesized by Bioneer Co. (Daejeon, Korea). DiO Cell-Labeling Solution was obtained from Thermo Fisher Scientific (Waltham, MA).

Blood-brain barrier hCMEC/D3 cells were acquired from Merck Millipore (Seoul, Korea). Human Astrocytes (HA) cells, Astrocyte Medium

(AM) kit, and endothelial cell medium (ECM) kit were purchased from ScienCell (Carlsbad, CA). Trypsin-EDTA was obtained from Gibco (Waltham, MA). DAPI and Phalloidin 594 were purchased from Sigma-Aldrich (St. Louis, MO). Lipid standard triacylglycerols (TG) (11:1-11:1-11:1) was obtained from Larodan Fine Chemicals AB (Solna, Sweden). Phosphatidylcholine (PC) (10:0-10:0), lysophosphatidylcholine (LPC) (13:0), phosphatidylethanolamine (PE) (10:0-10:0), lysophosphatidylethanolamine (LPE) (17:1), phosphatidic acid (PA) (10:0-10:0), lysophosphatidic acid (LPA) (17:0), phosphatidylinositol (PI) (8:0-8:0), lysophosphatidylinositol (LPI) (13:0), phosphatidylserine (PS) (10:0-10:0), and lysophosphatidylserine (LPS) (17:1) were purchased from Avanti Polar Lipids (Birmingham, AL).

**Methods: Plant-derived extracellular vesicle (pevs) and exosomes isolation:** Grapefruits were obtained from the local market and washed with a fruit cleaner and distilled water. Grapefruit juice was squeezed using a hand juicer. The initial total volume of the juice was 300 mL. To remove cellular debris and large particles, the juice was sequentially centrifuged 500 × g for 10 min, 3000 × g 30 min, and 10 000 × g 60 min at 4 °C, and the supernatant was collected. After 0.2 μm filtered, finally, ultracentrifugation (Ti75 rotor, Beckman Coulter, USA) was performed twice at 100 000 × g for 120 min. Grapefruit-derived pEV pellets were carefully resuspended in PBS, aliquoted, kept at −80 °C until use.

Exosome isolation from collected HA cell media was performed using the identical procedure as pEVs isolation. Large particles and cellular debris were eliminated through sequential centrifugation steps, consisting of 10 min 500 × g, 30 min 3000 × g, and 60 min 10 000 × g at 4 °C. The supernatant was collected, 0.2 μm filtered, and ultracentrifugation at 100 000 × g for 120 min was conducted twice. The HA exosome pellet was resuspended in PBS and preserved at −80 °C. The yields of the isolated pEVs and exosomes were measured using NTA.

**pEVs Characterization:** Prior to analysis, pEVs were diluted in filtered 1 × PBS (pH 7.4) to obtain an appropriate concentration before characterization. The size and zeta potential of pEV were measured using dynamic light scattering (Malvern Panalytical, Nano S90, UK) and a Zetasizer (Malvern Panalytical, Nano ZS, UK). The number of pEV was quantified using nanoparticle tracking analysis (Malvern Panalytical, LM10, UK). In addition, the morphology of pEV was characterized using cryogenic electron microscopy (FEI, Tecnai F20 G2, USA) after cryosampling.

**Lipidomics:** Three replicate samples of pEVs and HA cell-derived exosomes were used for lipidomic analysis. A two-step lipid extraction method was performed. An equal amount of pEV and exosome was added to a methanol/chloroform (2:1, v/v) solution containing lipid internal standard (IS) and vortexed three times for 30 s. After incubating for 10 min at 25 °C, the samples were centrifuged at 13 800 × g for 2 min at 4 °C. The supernatants were collected, and the remaining pellet was resuspended in chloroform/methanol/37% HCl (40:80:1, v/v/v), incubated for 15 min at 25 °C, and vortexed for 1 min with the addition of 250 μL of chloroform and 450 μL of 0.1 N HCl. Then, the samples were centrifuged at 6500 × g at 4 °C for 2 min, and the organic phase was collected from the bottom and pooled with the previously collected supernatants. After drying pooled samples, one half was dissolved in a mixture of 20 mM ammonium formate and 0.1% v/v formic acid in ACN: MeOH: water = 19:19:2 (solvent A) for positive and neutral lipid analysis, while the other half was dissolved in methanol for trimethylsilyldiazomethane (TMSD) methylation to analyze anionic lipids.

LC-MS analysis was performed using an HPLC (Agilent 1290 Infinity series, Agilent Technologies, Santa Clara, CA) coupled to a triple quadrupole mass spectrometer (QQQ LC-MS 6490 series, Agilent Technologies) equipped with a Hypersil Gold column (2.1 × 100 mm ID; 1.9 μm, Thermo Fisher Scientific) to separate the lipids. The lipid samples were separated using a mobile phase composed of solvent A and 20 mM ammonium formate and 0.1% v/v formic acid in 99% isopropyl alcohol. The column temperature was set at 40 °C, and the flow rate of the mobile phase was 250 μL min<sup>−1</sup>. All lipid samples were analyzed using multiple reaction monitoring (MRM) mode with computed transitions for each lipid class. The targeted lipids were assigned by comparing retention times with lipid internal standards. The Skyline software package (MacCoss Labora-

tory, Seattle, WA) was used to determine the peak area of each assigned lipid. All data were normalized by their respective internal standards.

**pEV-Aptamer Synthesis:** A hydrophobic insertion strategy and click chemistry were used to modify the surface of the pEVs with aptamers. Briefly, 0.5 mg of 1,2-distearoyl-*sn*-glycero-3-phosphoethanolamine-*N*-[maleimide (polyethylene glycol)–2000](DSPE-PEG(2000) maleimide) was dissolved in EtOH and incubated with 1 mg of pEV in PBS for 30 min at room temperature to form pEV-DSPE-PEG2000-Maleimide (pEV-Maleimide). Excess lipids were removed using a 100 kDa filter for further use. Before the 3' Thiol – R11-3 aptamer was attached, hydrophobic insertion of DSPE-PEG2000-Maleimide into pEV was assessed through Thiol-AAAAA-Cy5 incubated with washed pEV-maleimide at room temperature for 2 h. The aptamer R11-3 (CGAGUGCUUUUGAAUACUCUGGUUAGGGUCAUGCGGUUUUG) binding specifically to the BBB was 3' thiol modified, dissolved in TE buffer (final concentration 5 μM) and mixed with 1.0 N DTT solution. After incubation for 15 min at room temperature for reduction, DTT was removed by phase separation using ethyl acetate. Then, the mixture of pEV with the maleimide group and reduced 3' thiol-modified R11-3 aptamer was incubated at room temperature for 2 h for click chemistry. Purification of pEV-R11-3 was performed by dialysis (100 kDa dialysis tube) for 48 h with PBS to change the solvent. The size and concentration were then measured by DLS and NTA.

**Cell Culture:** The human brain endothelial cell line, hCMEC/D3, was obtained from Merck Millipore. The hCMEC/D3 cell line has been used to study drug carrier transport in the BBB. The cells were maintained at 37 °C with 5% CO<sub>2</sub> during culture and ECM containing 5% fetal bovine serum (FBS), 1% endothelial cell growth supplement (ECGS), 1% of antibiotic solution penicillin (P/S) were used. When hCMEC/D3 cell confluence reached 70%, the cells were washed with PBS, and subculture was performed routinely every 2 days under the same conditions.

Human astrocyte (HA) cells were acquired from ScienCell, and cultured according to the manufacturer's recommended protocol. The HA cells were cultured to obtain normal cell exosomes. The cells were maintained under humidified 5% CO<sub>2</sub> and 37 °C condition with astrocyte medium (AM) containing 2% exosome-depleted FBS, 1% of astrocyte growth supplement (AGS), 1% P/S solution. The HA cell media was collected for exosome isolation.

**Cellular Uptake of pEV-Aptamer Characterization:** Cellular uptake of pEV and their derivatives was investigated using confocal microscopy (LSM 700, Carl ZEISS). hCMEC/D3 cell line and U87MG cell lines were seeded into bottom-glass 24 confocal well plates at 1 × 10<sup>5</sup> cells per well, then incubated at 37 °C and 5% CO<sub>2</sub> overnight. After incubation, cells were washed with PBS. To visualize, DiO green fluorescent dye was labeled on pEV and pEV-Aptamer. A total of 1 × 10<sup>11</sup> particles mL<sup>−1</sup> of pEV, pEV-R11-3, and pEV-random, each 1 mL, were incubated with 4 μL of DiO dye solution for 25 min at 37 °C, followed by pEV isolation as described above to remove unbound DiO dye. The DiO-labeled pEV and pEV with R11-3 aptamer were mixed with cell media at a final concentration of 2 × 10<sup>9</sup> particles mL<sup>−1</sup>, and the cells were incubated for different periods (30 min, 1, 3, and 6 h). Then, the DiO-labeled pEVs in the ECM were removed by washing with PBS. hCMEC/D3 cells were fixed with 4% paraformaldehyde, and the nuclei of the cells were stained with 4',6-diamidino-2-phenylindole (DAPI, Sigma-Aldrich, Saint Louis, MO). hCMEC/D3 cell cytoskeleton was stained with 594-phalloidin (Sigma-Aldrich, St. Louis, MO). Confocal microscopy revealed that all fixed cell samples after treatment with pEV-R11-3. ImageJ software was used to quantify the intensity of internalized DiO labeled pEVs.

**Cell Viability Assay:** The viability of U87MG and hCMEC/D3 cells was assessed using WST Plus-8, a cell proliferation reagent. Briefly, 5 × 10<sup>3</sup> U87MG and hCMEC/D3 cells were seeded in a 96-well plate and incubated with different doses of the pEV-aptamer for 12 h. The cells were then pretreated with WST Plus-8 solution and incubated for 2 h. Absorbance was measured at 450 nm using a microplate reader.

**Quantification of pEVs uptake FACS (fluorescence-activated cell sorting) analysis:** Fluorescence-activated cell sorting (FACS) with CytoFLEX (Beckman Coulter, Indianapolis, USA) at 488 nm was used to study the hCMEC/D3 cellular uptake of the pEV-aptamer. Before cellular uptake,

hCMC/D3 cells were seeded in 12 well plates at a density of  $1 \times 10^5$  cells per well, then incubated overnight at 37 °C and 5% CO<sub>2</sub>. Then, the cells were washed twice with PBS, treated with DiO-labeled pEV and pEV-R11-3 aptamer at a final concentration of  $2 \times 10^9$  mL<sup>-1</sup>, and incubated for 3 h. After removing the media from each well, the cells were washed twice with PBS and detached with Trypsin EDTA. The detached cells were then centrifuged at 300 × g for 3 min and washed twice with PBS. Finally, after resuspending the cells in 600 μL PBS, fluorescence histograms were obtained immediately using a FACS machine.

**Preparation of DOX-Loaded pEVs:** To investigate the drug loading potential of pEV, we selected doxorubicin (DOX) as a model drug and performed a physical encapsulation technique using probe sonication. For loading DOX into pEV, the isolated pEVs ( $1 \times 10^{11}$  particles mL<sup>-1</sup>) were suspended in PBS with 180 μM doxorubicin, followed by probe sonication for 15 min (30 s on and 2 min off in an ice bath) at 20% amplitude using an ultrasonicator (Sonics, VC750, USA) to boost the influx of doxorubicin into the pEV membrane. Then the above mixture was incubated at 37 °C for 60 min to recover the exosome membranes. Finally, DOX-loaded pEVs were purified with PBS using a 100 kDa filter to remove unloaded free doxorubicin. DLS and NTA were used to measure the size distribution and particle concentration.

**In Vitro Drug Release:** The drug release profile of doxorubicin from the pEV nanocarrier was determined using 10 kDa dialysis. Briefly, 1 mL of pEV and DOX-loaded pEV was added to a 10 kDa dialysis tube. Then, the magnetic bar gently stirred the external PBS buffer, pH 7.4 and pH 5 at 37 °C to mimic the human body typical environment. At each time point, 100 μL of external buffer was collected to measure the fluorescence of doxorubicin using a microplate reader. The profile of drug release was quantified by measuring the fluorescence intensity of doxorubicin three times at each incubation time compared with the original doxorubicin fluorescence intensity.

**Statistical Analysis:** Statistical data are presented as mean ± standard deviation. The comparison between each sample group was analyzed with Student's *t*-test. *p* < 0.05 was considered a significant value. All experiments were conducted at least in triplicate and analyses were performed using GraphPad Prism v9.5.1 software (GraphPad Software, San Diego).

## Supporting Information

Supporting Information is available from the Wiley Online Library or from the author.

## Acknowledgements

This research was supported by the Korea Medical Device Development Fund grant funded by the Korean government (the Ministry of Science and ICT, the Ministry of Trade, Industry, and Energy, the Ministry of Health & Welfare, the Ministry of Food and Drug Safety) (KMDF\_PR\_20200901\_0072), and by the Nano-Connect Technology Research Program through the National Research Foundation of Korea (NRF), by Institute of Information & Communications Technology Planning & Evaluation (IITP) grant (2022-0-00159), funded by the Ministry of Science and ICT (NRF-2021M3H4A4079294) as well as by KIST internal grant program (Nos. 2E32232 and 2E32163). This work was supported by the Ministry of Trade, Industry and Energy grant funded by the Korea government (No. 20018522), and by the Research Institute for Convergence Science. The authors thank Dr. Hyun Mee, Park for her assistance with lipidomics.

## Conflict Of Interest

The authors declare no conflict of interest.

## Data Availability Statement

The data that support the findings of this study are available from the corresponding author upon reasonable request.

## Keywords

drug delivery carrier, plant-derived extracellular vesicle, targeted delivery

Received: March 15, 2023

Revised: May 11, 2023

Published online: July 13, 2023

- [1] S. Cunha, B. Forbes, J. M. Sousa Lobo, A. C. Silva, *Int. J. Nanomed.* **2021**, *16*, 4373.
- [2] R. Taliyan, V. Kakoty, K. C. Sarathlal, S. S. Kharavtekar, C. R. Karennavar, Y. K. Choudhary, G. Singhvi, Y. Riadi, S. K. Dubey, P. Kesharwani, *J. Controlled Release* **2022**, *343*, 528.
- [3] X. W. Dong, *Theranostics* **2018**, *8*, 1481.
- [4] J. J. E. Mulvihill, E. M. Cunnane, A. M. Ross, J. T. Duskey, G. Tosi, A. M. Grabrucker, *Nanomedicine* **2020**, *15*, 205.
- [5] K. Lingineni, V. Belekar, S. R. Tangadpalliwar, P. Garg, *Mol. Divers.* **2017**, *21*, 355.
- [6] W. M. Pardridge, *J. Cereb. Blood Flow Metab.* **2012**, *32*, 1959.
- [7] R. Kalluri, V. S. LeBleu, *Science* **2020**, *367*, 6478.
- [8] T. Tian, H. X. Zhang, C. P. He, S. Fan, Y. L. Zhu, C. Qi, N. P. Huang, Z. D. Xiao, Z. H. Lu, B. A. Tannous, J. Gao, *Biomaterials* **2018**, *150*, 137.
- [9] L. van der Koog, T. B. Gandek, A. Nagelkerke, *Adv. Healthcare Mater.* **2022**, *11*, 2100639.
- [10] T. Yang, P. Martin, B. Fogarty, A. Brown, K. Schurman, R. Phipps, V. P. Yin, P. Lockman, S. Bai, *Pharm. Res.* **2015**, *32*, 2003.
- [11] M. Xu, Q. Yang, X. Sun, Y. Wang, *Front. Bioeng. Biotechnol.* **2020**, *8*, 586130.
- [12] C. C. Chen, L. Liu, F. Ma, C. W. Wong, X. E. Guo, J. V. Chacko, H. P. Farhoodi, S. X. Zhang, J. Zimak, A. Ségaliny, M. Riazifar, V. Pham, M. A. Digma, E. J. Pone, W. Zhao, *Cell. Mol. Bioeng.* **2016**, *9*, 509.
- [13] T. A. Druzhkova, A. A. Yakovlev, *Neurochem. J.* **2018**, *12*, 195.
- [14] M. Khongkow, T. Yata, S. Boonrungsiman, U. R. Ruktanonchai, D. Graham, K. Namdee, *Sci. Rep.* **2019**, *9*, 8278.
- [15] S. F. Liang, H. Y. Xu, B. C. Ye, *Langmuir* **2022**, *38*, 299.
- [16] I. K. Herrmann, M. J. A. Wood, G. Fuhrmann, *Nat. Nanotechnol.* **2021**, *16*, 748.
- [17] J. Ahlawat, G. Guillama Barroso, S. Masoudi Asil, M. Alvarado, I. Armendariz, J. Bernal, X. Carabaza, S. Chavez, P. Cruz, V. Escalante, S. Estorga, D. Fernandez, C. Lozano, M. Marrufo, N. Ahmad, S. Negrete, K. Olvera, X. Parada, B. Portillo, A. Ramirez, R. Ramos, V. Rodriguez, P. Rojas, J. Romero, D. Suarez, G. Urueta, S. Viel, M. Narayan, *ACS Omega* **2020**, *5*, 12583.
- [18] C. X. Chen, M. Sun, J. Wang, L. Su, J. Lin, X. Yan, *J. Extracell. Vesicles* **2021**, *10*, e12163.
- [19] H. A. Dad, T. W. Gu, A. Q. Zhu, L. Q. Huang, L. H. Peng, *Mol. Ther.* **2021**, *29*, 13.
- [20] Y. Cui, J. Gao, Y. He, L. Jiang, *Protoplasma* **2020**, *257*, 3.
- [21] N. Kameli, A. Dragojlovic-Kerkache, P. Savelkoul, F. R. Stassen, *Membranes* **2021**, *11*, 411.
- [22] M. Nemati, B. Singh, R. A. Mir, M. Nemati, A. Babaei, M. Ahmadi, Y. Rasmi, A. G. Golezani, J. Rezaie, *Cell Commun. Signaling* **2022**, *20*, 69.
- [23] M. Q. Lian, W. H. Chng, J. Liang, H. Q. Yeo, C. K. Lee, M. Belaid, M. Tollemeto, M. G. Wacker, B. Czarny, G. Pastorin, *J. Extracell. Vesicles* **2022**, *11*, 12283.
- [24] S. Gurung, D. Perocheau, L. Touramanidou, J. Baruteau, *Cell Commun. Signaling* **2021**, *19*, 47.

- [25] Q. L. Wang, X. Y. Zhuang, J. Y. Mu, Z. B. Deng, H. Jiang, L. F. Zhang, X. Y. Xiang, B. M. Wang, J. Yan, D. Miller, H. G. Zhang, *Nat. Commun.* **2013**, *4*, 1867.
- [26] Q. Wang, Y. Ren, J. Mu, N. K. Egilmez, X. Zhuang, Z. Deng, L. Zhang, J. Yan, D. Miller, H. G. Zhang, *Cancer Res.* **2015**, *75*, 2520.
- [27] B. Jing, Y. Gai, R. Qian, Z. Liu, Z. Zhu, Y. Gao, X. Lan, R. An, *J. Nanobiotechnol.* **2021**, *19*, 7.
- [28] T. Smyth, K. Petrova, N. M. Payton, I. Persaud, J. S. Redzic, M. W. Graner, P. Smith-Jones, T. J. Anchordoquy, *Bioconjug. Chem.* **2014**, *25*, 1777.
- [29] P. Dua, S. Kang, H. S. Shin, S. Kim, D. K. Lee, *Nucl. Acid Ther.* **2018**, *28*, 262.
- [30] M. Paulaitis, K. Agarwal, P. Nana-Sinkam, *Langmuir* **2018**, *34*, 9387.
- [31] S. Gurunathan, M. H. Kang, M. Jeyaraj, M. Qasim, J. H. Kim, *Cells* **2019**, *8*, 307.
- [32] G. Midekessa, K. Godakumara, J. Ord, J. Viil, F. Lättekivi, K. Dissanayake, S. Kopanchuk, A. Rincken, A. Andronowska, S. Bhattacharjee, T. Rincken, A. Fazeli, *ACS Omega* **2020**, *5*, 16701.
- [33] W. M. Huang, X. Wu, X. Gao, Y. Yu, H. Lei, Z. Zhu, Y. Shi, Y. Chen, M. Qin, W. Wang, Y. Cao, *Nat. Chem.* **2019**, *11*, 310.
- [34] R. L. Li, Y. Wu, Z. Bai, J. Guo, X. Chen, *RSC Adv.* **2020**, *10*, 42120.
- [35] M. Li, S. Jiang, J. Simon, D. Paßlick, M. L. Frey, M. Wagner, V. Mailänder, D. Crespy, K. Landfester, *Nano Lett.* **2021**, *21*, 1591.
- [36] G. Zhu, X. Chen, *Adv. Drug Delivery Rev.* **2018**, *134*, 65.
- [37] J. A. Mindell, *Annu. Rev. Physiol.* **2012**, *74*, 69.
- [38] H. Wei, J. Chen, S. Wang, F. Fu, X. Zhu, C. Wu, Z. Liu, G. Zhong, J. Lin, *Int. J. Nanomed.* **2019**, *14*, 8603.
- [39] J. Lee, J. H. Lee, K. Chakraborty, J. Hwang, Y. K. Lee, *RSC Adv.* **2022**, *12*, 18475.